ADVANCING EARTH AND SPACE SCIENCES

JGR Space Physics

RESEARCH ARTICLE
10.1029/2026JA035515

Key Points:

- The time evolution of electron-only reconnection has been investigated both in the keda linear magnetized plasma (KLMP) device and in a dedicated particle-in-cell (PIC) simulation
- The dedicated PIC simulation demonstrates the absence of obvious ion outflow caused by reconnection process
- The electron dynamics responsible for the Hall magnetic field, as observed in the KLMP device and simulation, is elucidated

Supporting Information:

Supporting Information may be found in the online version of this article.

Correspondence to:
Q. Lu,
qmlu@ustc.edu.cn

Citation:
Hu, S., Yang, F., Lu, Q., Zhang, Q., Xie, J., Gao, X., et al. (2026). Electron-only magnetic reconnection in keda linear magnetized plasma (KLMP) device: Comparison between laboratory study and kinetic simulation. *Journal of Geophysical Research: Space Physics*, *131*, e2026JA035515. https://doi.org/10.1029/2026JA035515

Received 14 APR 2026
Accepted 8 JUL 2026

Electron-Only Magnetic Reconnection in Keda Linear Magnetized Plasma (KLMP) Device: Comparison Between Laboratory Study and Kinetic Simulation

Shihang Hu[1,2], Fa Yang[1,2], Quanming Lu[1,2], Qiaofeng Zhang[1,2], Jinlin Xie[3], Xinliang Gao[1,2], Yangguang Ke[1,2], Yukang Shu[1,2], Youran Liu[3], Longlong Sang[1], San Lu[1,2], Rongsheng Wang[1,2], and Weixing Ding[3]

[1]Deep Space Exploration Laboratory, School of Earth and Space Sciences, University of Science and Technology of China, Hefei, China, [2]Collaborative Innovation Center of Astronautical Science and Technology, Harbin, China, [3]School of Nuclear Science and Technology, University of Science and Technology of China, Hefei, China

Abstract Electron-only magnetic reconnection, a new type of magnetic reconnection characterized by the absence of obvious ion outflow and heating, has been widely studied by in situ spacecraft observations in space plasma. This paper presents an experimental investigation of electron-only magnetic reconnection in the Keda Linear Magnetized Plasma (KLMP) device, complemented by a dedicated particle-in-cell (PIC) simulation. When reversed magnetic fields generated by two parallel aluminum rods approach and compress each other, a current sheet forms with a width on the order of the electron inertial length. Magnetic reconnection with a strong guide field subsequently occurs in this current sheet, and the Hall magnetic field with a distorted quadrupolar structure is measured. The PIC simulation demonstrates that the current is carried mainly by the electrons, that the reconnection process does not produce obvious ion outflow. These results indicate that electron-only magnetic reconnection has been successfully realized in the KLMP device.

Plain Language Summary Magnetic reconnection is a process where magnetic field lines break and reconnect, releasing stored magnetic energy to heat and accelerate particles. Recently, a new type called electron-only reconnection has been discovered in space, in which ions remain unresponsive to the reconnection process. To better understand this process, we reproduced it in a laboratory device called the Keda Linear Magnetized Plasma. In experiment, two parallel metal rods generate magnetic fields that push against each other, creating a thin current sheet where reconnection occurs. We also used a computer simulation to model the same process. The simulation successfully reproduces the experimental results and confirms that the reconnection is indeed electron-only reconnection. In addition, the simulation helps explain how the motions of electrons give rise to the characteristic magnetic field structures observed in the experiment. This combined experimental and computational approach provides a clearer picture of electron-only reconnection, a process frequently observed in Earth's magnetosphere and other space environments.

1. Introduction

Magnetic reconnection is a fundamental plasma process that rearranges magnetic field line topologies and converts magnetic energy into particle energy (Biskamp, 2000; Yamada et al., 2010). It plays a key role in energizing particles and driving explosive phenomena across diverse plasma environments. These include the solar atmosphere (Cassak & Shay, 2012; Krucker et al., 2010; Masuda et al., 1994), interplanetary space (Gosling et al., 2005; R. Wang et al., 2023; Z. Wang et al., 2023; Wei et al., 2003), planetary magnetospheres (Dai et al., 2024; Q. Lu et al., 2022; Øieroset et al., 2001; R. Wang et al., 2010; R. Wang et al., 2024; S. Wang et al., 2024; Zhang et al., 2012), as well as laboratory experiments (Dong et al., 2012; Egedal et al., 2007; Frank, 1999, 2025; Huang et al., 2025; Li et al., 2007; Yamada et al., 2006, 2015; Yang et al., 2025). The standard collisionless magnetic reconnection model features a two-scale structure, comprising the ion diffusion region (IDR) at the scale of the ion inertial length and the electron diffusion region (EDR) at the scale of the electron inertial length (Birn et al., 2001; Chang et al., 2024; Kleva et al., 1995; Q. Lu et al., 2010; Ma & Bhattacharjee, 2001; Øieroset et al., 2001; Pritchett, 2001; Zhou et al., 2019). In the IDR, the electrons are magnetized, while the ions are demagnetized. In the EDR, which is embedded in the IDR, the electron motions also become demagnetized.

10.1029/2026JA035515

Recently, a new type of magnetic reconnection, electron-only magnetic reconnection, has been observed in Earth's magnetosphere (Hubbert et al., 2021, 2022; S. Lu et al., 2020; Man et al., 2020; Phan et al., 2018; R. Wang et al., 2018, 2020). Electron-only reconnection usually occurs in an electron current sheet where the current is predominantly carried by electrons, with its width on the order of the electron inertial length. Different from standard reconnection, electron-only reconnection exhibits only the electron dynamics, while ions remain unresponsive to the reconnection process. As a result, there is no significant ion outflow or heating observed. The magnetic energy released during reconnection is predominantly converted into the kinetic and thermal energy of electrons (Guan et al., 2023, 2024, 2025; S. Lu et al., 2022; Pyakurel et al., 2019; Roy et al., 2024). Furthermore, one pronounced feature of electron-only reconnection is the higher reconnection rate than standard reconnection, signifying a more efficient release of magnetic energy (Guan et al., 2023; Liu et al., 2025; Q. Lu et al., 2025; Pyakurel et al., 2019).

In addition to observations in space plasmas, the physical mechanisms of electron-only reconnection have also been directly verified and studied under controlled laboratory conditions (Greess et al., 2021, 2022; Nirwan et al., 2025; Rovige et al., 2024, 2026; Sakai et al., 2022; Shi et al., 2022a, 2022b, 2023; Yang et al., 2025). In Yang et al. (2025), the realization of electron-only reconnection with a guide field in the Keda Linear Magnetized Plasma (KLMP) device has been reported. In the KLMP experiment, both the spatial and temporal scales are confined to the electron scale, and a quadrupolar structure of Hall magnetic field, as well as electron heating, are identified. However, conclusive observational proof for electron-only reconnection was lacking in Yang et al. (2025). Therefore, in this paper, we perform a particle-in-cell (PIC) simulation to model the physical process observed in the KLMP experiment. A detailed comparison between the experimental and simulation results reveals excellent agreement. Furthermore, the simulation results confirm that the physical process observed in the KLMP device is indeed electron-only reconnection, rather than standard reconnection.

2. Experimental and Simulation Setup

The KLMP experiment is modeled via a kinetic, two-dimensional (2D) PIC simulation conducted with the EPOCH code (Arber et al., 2015) in the *x*-*z* plane. Experimental details can be found in Yang et al. (2025) or the Supporting Information S1. Under the experimental plasma conditions, the peak plasma density is approximately $1 \times 10^{12}\,\mathrm{cm}^{-3}$, the electron temperature T_e is about 5 eV, and the ion temperature T_i is roughly 0.1 times the electron temperature. Accordingly, the density in the simulation is normalized to $n_0 = 1 \times 10^{12}\,\mathrm{cm}^{-3}$, and the magnetic field is normalized to $B_0 = 15\,\mathrm{Gs}$. This normalization field is determined by equating the magnetic pressure to the maximum thermal pressure of the plasma: $B_0^2/(2\mu_0) = n_0 k_B (T_e + T_i)$. A full list of normalized parameters and their reference values is provided in Table S1 in Supporting Information S1.

Magnetic reconnection occurs in the presence of a guide field $B_g = 4B_0$. The working gas in KLMP is argon (Ar), corresponding to a mass ratio of $m_i/m_e = 1836 \times 40$ used in the simulation. The dominant collisions among plasma particles are electron-electron and electron-ion collisions, with normalized frequencies $\nu_{ei}/\omega_{ce} = \nu_{ee}/\omega_{ce} \approx 2.97 \times 10^{-3}$. For electron-neutral interactions, the dominant process is elastic scattering between electrons and Ar atoms, with $\nu_{en}/\omega_{ce} \approx 9.18 \times 10^{-4}$, where $\omega_{ce} = eB_g/m_e \approx 1.06 \times 10^9\,\mathrm{s}^{-1}$. Therefore, a collisionless PIC simulation is sufficient to model the system. Regarding boundary conditions, we theoretically computed the return current on the vacuum chamber wall to ensure that the magnetic field lines are tangential to the chamber wall, that is, a conducting boundary condition. Meanwhile, the plasma is absorbed and removed from the simulation domain upon reaching the vacuum chamber wall (and the current-carrying rods). Further details on the simulation setup are provided in Supporting Information S1. It should be noted that although magnetic reconnection in the KLMP is inherently three-dimensional (3D), the PIC simulation used here is 2D. To better reproduce the experimental physics in the simulation, at each time step, particles that have accumulated an out-of-plane displacement exceeding $120d_e$ are reset, with their new velocities sampled from a Maxwellian distribution at the initial temperature. Here, $120d_e$ corresponds to half the length of the current-carrying rods in the experiment. This approach effectively emulates the experimental condition: particles that leave the reconnection region along the out-of-plane direction are replenished by incoming particles, rather than being continuously accelerated by the reconnection electric field.

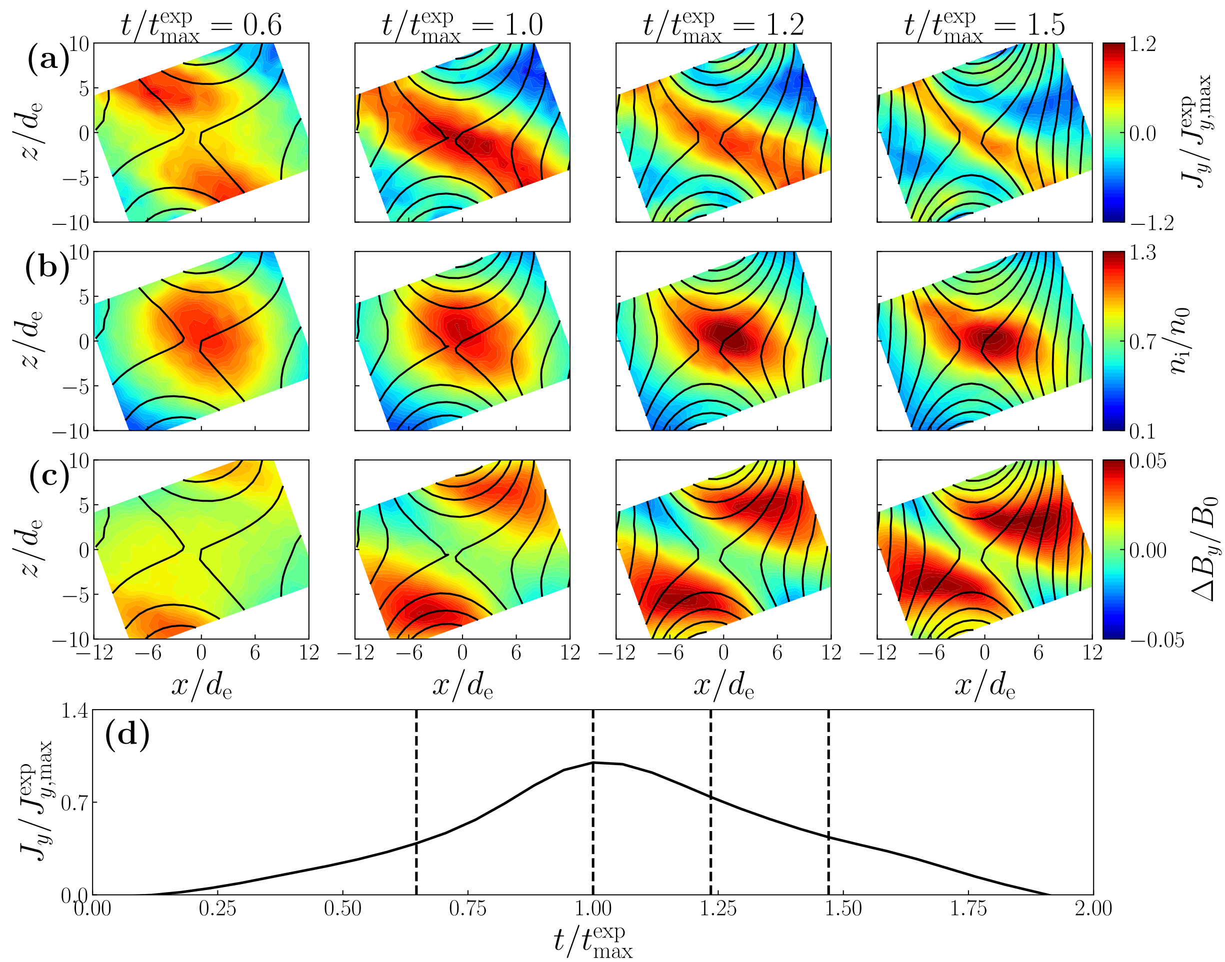

Figure 1. Temporal evolution, as measured in the keda linear magnetized plasma experiment, of (a) the out-of-plane current density J_y, (b) the ion density n_i, and (c) the Hall magnetic field $\Delta B_y = B_y(t) - B_y(t = 0)$ at $t/t_{max}^{exp} = 0.6$, 1.0, 1.2, and 1.5. (d) shows the temporal evolution of the out-of-plane current density J_y at the X-line. Here, t_{max}^{exp} and $J_{y,max}^{exp}$ represent the time and the current magnitude at which J_y reaches its maximum.

3. Results

Figures 1 and 2 present the experimental and simulation results, respectively, allowing for comparison. Figure 1 shows the temporal evolution, as measured in the KLMP experiment, of (a) the out-of-plane current density J_y, (b) the ion density n_i, and (c) the Hall magnetic field $\Delta B_y = B_y(t) - B_y(t = 0)$ at $t/t_{max}^{exp} = 0.6$, 1.0, 1.2, and 1.5. Figure 1d shows the temporal evolution of the out-of-plane current density J_y at the X-line, where t_{max}^{exp} and $J_{y,max}^{exp}$ represent the time and the current magnitude at which J_y reaches its maximum. Figure 2 presents the same set of physical parameters, but with data obtained from the simulation. Furthermore, due to the absence of a distinct peak, the values for t_{max}^{sim} and $J_{y,max}^{sim}$ are determined by taking the average over the plateau region (blue-shaded area) in Figure 2d, representing the characteristic time and magnitude of J_y. The experiment and simulation reveal similar physical processes. Initially, two parallel aluminum rods generate reversed magnetic fields. As these fields approach and compress each other, a current sheet forms with a width on the order of the electron inertial length. Magnetic reconnection with a strong guide field subsequently occurs in this current sheet. The current sheet exhibits distinct spatial and temporal characteristics: Spatially, it is distributed along the separatrix extending from the upper-left to the lower-right; Temporally, the current density J_y first increases to a peak and then decays. Throughout the reconnection process, the plasma density near the X-line increases. Meanwhile, the distorted quadrupolar Hall magnetic field also develops. It exhibits larger triangular regions of positive ΔB_y, with smaller regions of negative ΔB_y near the upper-left and lower-right separatrix. In addition to the consistency in physical processes, a quantitative comparison between the experiment and simulation is presented below. The measured

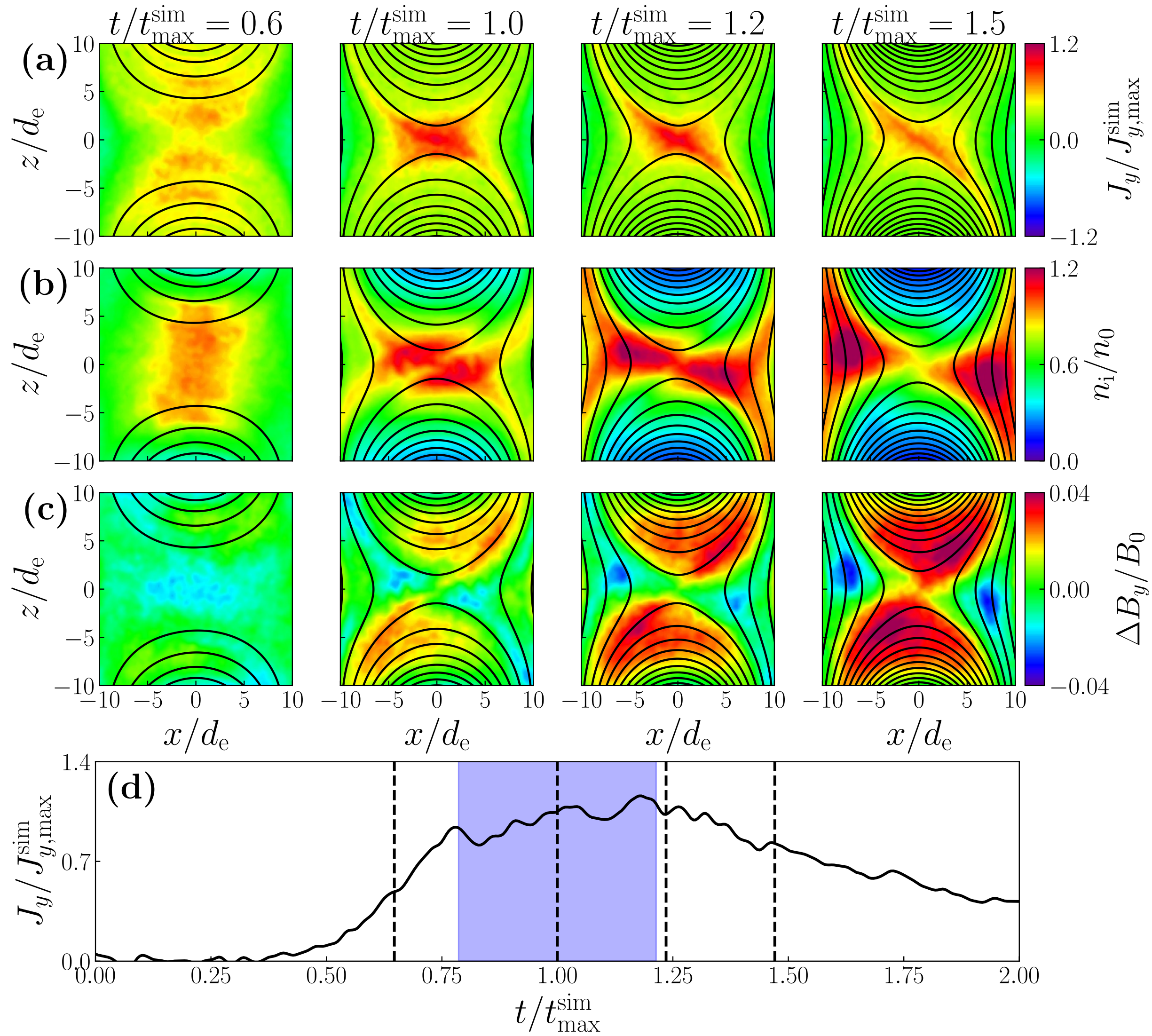

Figure 2. Temporal evolution, as obtained from the simulation, of (a) the out-of-plane current density J_y, (b) the ion density n_i, and (c) the Hall magnetic field $\Delta B_y = B_y(t) - B_y(t = 0)$ at $t/t_{max}^{sim} = 0.6$, 1.0, 1.2, and 1.5. (d) shows the temporal evolution of the out-of-plane current density J_y at the X-line. Here, t_{max}^{sim} and $J_{y,max}^{sim}$ represent the characteristic time and current magnitude, determined by averaging over the plateau region in (d).

and simulated Hall magnetic fields are comparable, both around $0.04B_0 \sim 0.05B_0$. However, the characteristic time from the simulation, $t_{max}^{sim} = 3.7 \times 10^3\ \Omega_e^{-1}$, is 1.7 times that of the experiment, $t_{max}^{exp} = 2.2 \times 10^3\ \Omega_e^{-1}$; the characteristic current density from the simulation, $J_{y,max}^{sim} = 35.4\, n_0 e V_A$, is 2.8 times that of the experiment, $J_{y,max}^{exp} = 12.6\, n_0 e V_A$.

Given that both the spatial and temporal scales are confined to the electron scale, the process observed in KLMP is identified as electron-only reconnection (Yang et al., 2025). However, conclusive observational proof has been absent. To verify this, Figure 3 shows the temporal evolution, as obtained from the simulation, of (a) the out-of-plane electron current density J_{ey}, (b) the out-of-plane ion current density J_{iy}, (c) the electron bulk velocity V_{ex}, and (d) the ion bulk velocity V_{ix} at $t/t_{max}^{sim} = 0.6$, 1.0, 1.2, and 1.5. The out-of-plane ion current density J_{iy} is three orders of magnitude smaller than the out-of-plane electron current density J_{ey}, indicating that the current is predominantly carried by electrons. This identifies the process as electron-only reconnection. However, the process exhibits a weak yet non-negligible ion outflow V_{ix}, which is one order of magnitude smaller than the electron outflow V_{ex}. This appears inconsistent with the understanding that no significant ion outflow exists in

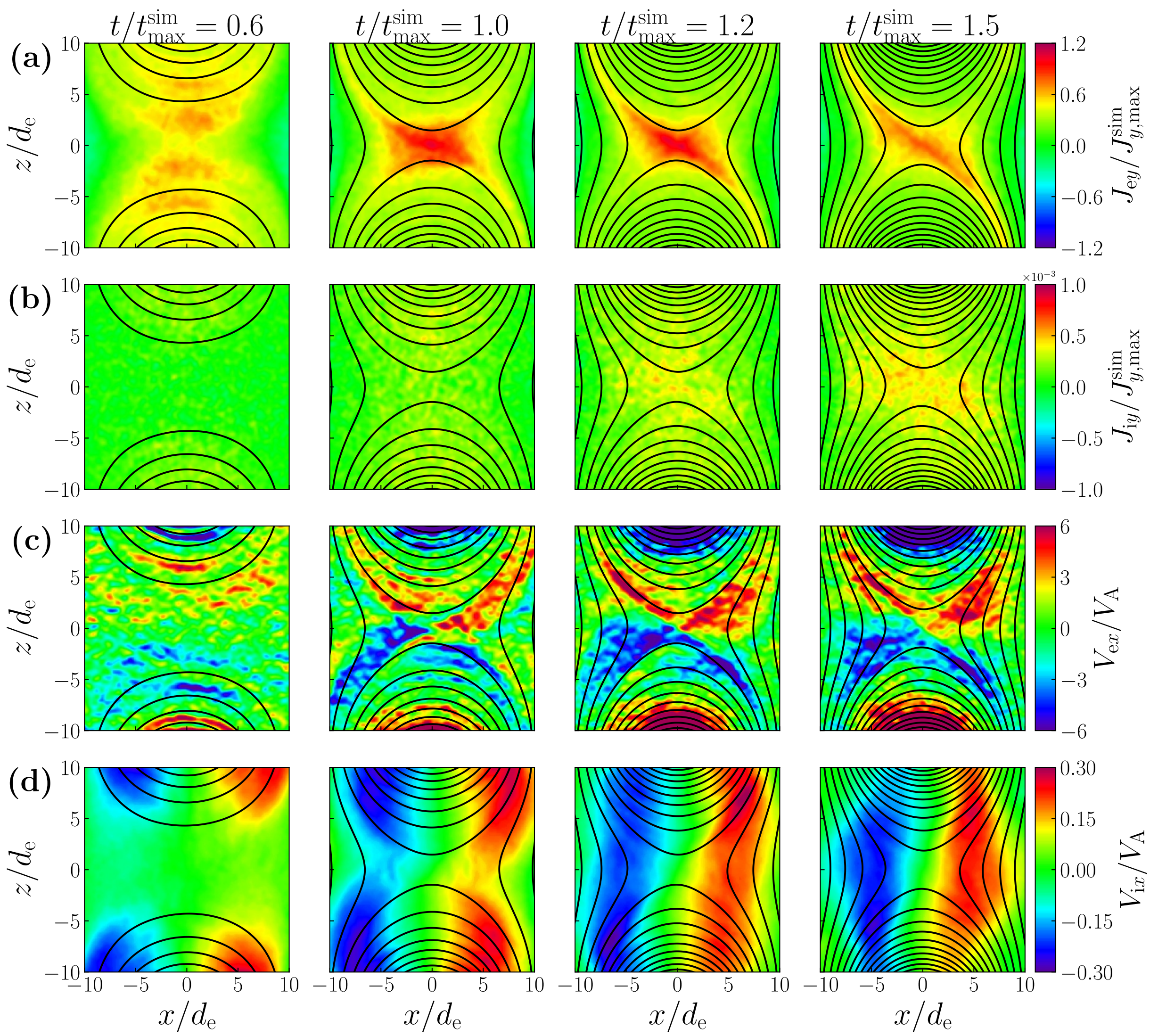

Figure 3. Temporal evolution, as obtained from the simulation, of (a) the out-of-plane electron current density J_{ey}, (b) the out-of-plane ion current density J_{iy}, (c) the electron bulk velocity V_{ex}, and (d) the ion bulk velocity V_{ix} at $t/t_{max}^{sim} = 0.6$, 1.0, 1.2, and 1.5.

electron-only reconnection. Further examination reveals that an ion outflow is already detectable at $t/t_{max}^{sim} = 0.6$, a time when magnetic reconnection has not been triggered, and it is not localized around the X-line. This suggests that the observed ion outflow is not caused by magnetic reconnection. Consequently, despite the observed weak ion outflow, the process remains classified as electron-only reconnection.

To provide additional support for this conclusion, Figure 4 shows the resultant force on ions and the contributions of its three components at $t/t_{max}^{sim} = 1.2$, as expressed by

$$m_i \frac{dV_{ix}}{dt} = \underbrace{e\boldsymbol{E}}_{\boldsymbol{F}_{i,1}} + \underbrace{e\boldsymbol{V}_i \times \boldsymbol{B}}_{\boldsymbol{F}_{i,2}} \underbrace{-\frac{1}{n_i}\nabla \cdot \boldsymbol{P}_i}_{\boldsymbol{F}_{i,3}}. \tag{1}$$

It can be observed that the force on the ions $m_i \frac{dV_{ix}}{dt}$ comes primarily from the electric field force $\boldsymbol{F}_{i,1}$ and the pressure gradient force $\boldsymbol{F}_{i,3}$, while the contribution from the Lorentz force $\boldsymbol{F}_{i,2}$ (macroscopically, the Ampere force, i.e., the volume integral of the Lorentz force) is negligible. This aligns with the previous conclusion that the ion outflow does not originate from reconnection. The pressure gradient force arises from the density gradient as

10.1029/2026JA035515

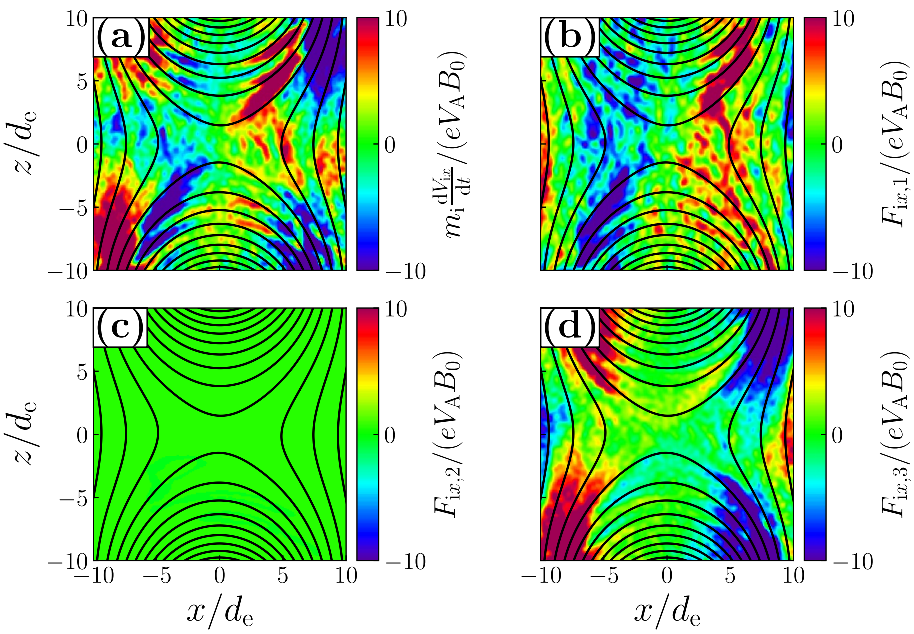

Figure 4. (a) The resultant force on ions, $m_\mathrm{i}\frac{\mathrm{d}V_{\mathrm{i}x}}{\mathrm{d}t}$, as obtained from the simulation at $t/t_{\max}^{\mathrm{sim}} = 1.2$. The contributions of its three components are shown in (b)–(d): the electric field force $\boldsymbol{F}_{\mathrm{i},1} = e\boldsymbol{E}$, the Lorentz force $\boldsymbol{F}_{\mathrm{i},2} = e\boldsymbol{V}_\mathrm{i} \times \boldsymbol{B}$, and the pressure gradient force $\boldsymbol{F}_{\mathrm{i},3} = -\frac{1}{n_\mathrm{i}}\nabla \cdot \boldsymbol{P}_\mathrm{i}$.

shown in Figure 2b, and the electric field originates from charge separation through the following process. When a driving current is applied to the current-carrying rods, a non-uniform magnetic field is generated, producing a magnetic pressure gradient force $-\nabla B^2/(2\mu_0)$ that pushes the plasma away from the rods. During this process, due to their much smaller mass, electrons are more easily accelerated, resulting in charge separation and the establishment of an electric field. This electric field then pulls the ions along, causing them to move away from the rods as well. Therefore, the ion bulk velocity is a consequence of the driving source (the current-carrying rods). It follows that even with a single current-carrying rod (where no reconnection occurs), an ion bulk velocity can still be generated.

In Yang et al. (2025), we reported the observation of a distorted quadrupolar Hall magnetic field in KLMP. Here, drawing on the simulation results presented in Figure 5, we further analyze this structure. Figures 5a and 5b show the Hall magnetic field ΔB_y and the electron bulk velocity $V_{\mathrm{e}x}$ at $t/t_{\max}^{\mathrm{sim}} = 1.2$. Due to the low bulk velocity of the ions, the Hall current, which generates the Hall magnetic field, is primarily carried by electrons. Taking the region with $z < 0$ as an example, the positive ΔB_y triangle is primarily generated by two distinct electron flows: negative $V_{\mathrm{e}x}$ in the separatrix region and positive $V_{\mathrm{e}x}$ in the inflow region. To analyze the electron dynamics, we consider the electron momentum equation. Given the negligible electron mass, the inertial term is omitted, yielding:

$$0 = -e(\boldsymbol{E} + \boldsymbol{V}_\mathrm{e} \times \boldsymbol{B}) - \frac{1}{n_\mathrm{e}}\nabla \cdot \boldsymbol{P}_\mathrm{e}. \tag{2}$$

Taking the cross product of Equation 2 with $\boldsymbol{e}_y$ and then dividing by B_y yields:

$$\boldsymbol{V}_\mathrm{e} = \underbrace{\frac{V_{\mathrm{e}y}}{B_y}\boldsymbol{B}}_{\boldsymbol{V}_{\mathrm{e},1}} + \underbrace{\frac{\boldsymbol{E} \times (B_y\mathbf{e}_y)}{B_y^2}}_{\boldsymbol{V}_{\mathrm{e},2}} + \underbrace{\frac{\nabla \cdot \boldsymbol{P}_\mathrm{e} \times (B_y\mathbf{e}_y)}{n_\mathrm{e}eB_y^2}}_{\boldsymbol{V}_{\mathrm{e},3}}. \tag{3}$$

Figure 5c demonstrates that $V_{\mathrm{e}x} - \sum_{i=1}^{3} V_{\mathrm{e}x,i}$ is essentially zero, which justifies the neglect of the electron inertia term. Figures 5d–5f present the three components of the electron bulk velocity: the field-aligned motion $\boldsymbol{V}_{\mathrm{e},1}$, the E × B drift $\boldsymbol{V}_{\mathrm{e},2}$, and the diamagnetic drift $\boldsymbol{V}_{\mathrm{e},3}$. This decomposition clarifies the electron dynamics responsible

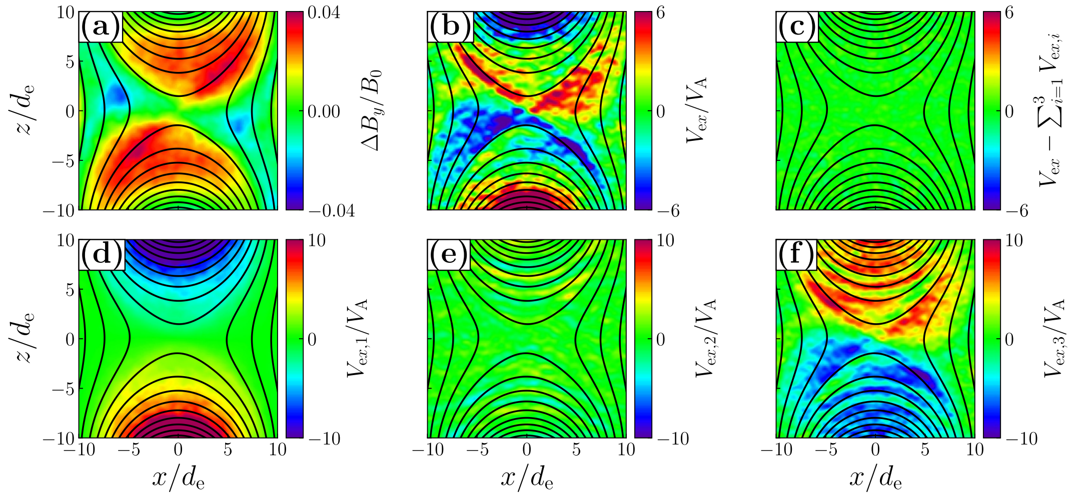

Figure 5. (a) and (b) show the Hall magnetic field ΔB_y and the electron bulk velocity V_{ex}, as obtained from the simulation at $t/t_{max}^{sim} = 1.2$. (c) shows the residual $V_{ex} - \sum_{i=1}^{3} V_{ex,i}$, where $V_{ex,i}$ denote three components contributing to the electron bulk velocity: $\boldsymbol{V}_{e,1} = \frac{V_{ey}}{B_y}\boldsymbol{B}$; $\boldsymbol{V}_{e,2} = \frac{\boldsymbol{E}\times(B_y\boldsymbol{e}_y)}{B_y^2}$; and $\boldsymbol{V}_{e,3} = \frac{\nabla\cdot\boldsymbol{P}_e\times(B_y\boldsymbol{e}_y)}{neB_y^2}$. These three components $V_{ex,i}$ are shown in (d)–(f).

for the Hall magnetic field. The E × B drift contribution $V_{ex,2}$ is negligible. In the separatrix region, the electron bulk velocity V_{ex} is primarily contributed by the diamagnetic drift $V_{ex,3}$, which arises from the presence of density gradient as shown in Figure 2b. In contrast, in the inflow region, where B_x is relatively large owing to the proximity to the current-carrying rods, the dominant contribution to the electron bulk velocity V_{ex} comes from the field-aligned motion $V_{ex,1}$. Importantly, to avoid any circular reasoning (i.e., using the Hall field ΔB_y to explain itself), we emphasize that this decomposition is physically meaningful only in the presence of a strong guide field, where $B_y \approx B_g$ is essentially unaffected by the Hall magnetic field.

4. Conclusions and Discussion

This paper presents an experimental investigation of electron-only magnetic reconnection in the KLMP device, complemented by a dedicated particle-in-cell (PIC) simulation. The time evolution of reconnection in the experiment and simulation is compared, and good consistency is confirmed. When reversed magnetic fields generated by two parallel aluminum rods approach and compress each other, a current sheet forms with a width on the order of the electron inertial length. Magnetic reconnection with a strong guide field subsequently occurs in this current sheet, and the Hall magnetic field with a distorted quadrupolar structure is measured. The PIC simulation demonstrates that the current sheet is predominantly carried by electrons, and the ion outflow caused by reconnection process is absent. This indicates that electron-only magnetic reconnection has been successfully realized in the KLMP device. Additionally, we elucidate the electron dynamics responsible for the observed Hall magnetic field in Yang et al. (2025).

This study employs PIC simulation to further investigate the electron-only reconnection occurring in KLMP. While the simulation captures the key physics, certain discrepancies with experimental results remain. Numerically, the ratios $t_{max}^{sim}/t_{max}^{exp} = 1.7$ and $J_{y,max}^{sim}/J_{y,max}^{exp} = 2.8$ are somewhat large. Physically, the negative out-of-plane current observed in the experimental results (Figure 1a) does not appear in the simulation results (Figure 2a). The primary source of these discrepancies lies in the dimensionality of the model: simulations are conducted in 2D, whereas the actual KLMP reconnection is a 3D process. Although the velocities of particles satisfying specific criteria are reset at each time step, the electrostatic field in the out-of-plane direction is absent in 2D simulation. Furthermore, to maintain quasi-neutrality, electrons in KLMP that flow from the source region toward the ends subsequently return toward the source. This process results in the negative out-of-plane current observed in the experiment, a feature that the 2D simulation cannot replicate. Nevertheless, the numerical discrepancies remain within a reasonable range, and the negative out-of-plane current is not part of the reconnection process under investigation. Therefore, the simulation still captures the essential physics of reconnection in KLMP.

Electron-only reconnection is routinely observed in Earth's magnetosphere. Yet single-point measurements cannot resolve the two-dimensional structure, nor can they unambiguously distinguish the effects of external driving from intrinsic reconnection dynamics. The combination of laboratory experiment and kinetic simulation presented here provides complementary insights that can aid in interpreting MMS observations and future missions. Under the strong guide-field condition–which is typical of many space plasma environments–our analysis further reveals that the distorted Hall field arises from electron diamagnetic drift and field-aligned motion, underscoring the essential role of electron dynamics. Therefore, the physical insights gained from this work are broadly applicable to understanding magnetic energy release in space plasmas.

Conflict of Interest

The authors declare no conflicts of interest relevant to this study.

Availability Statement

The experimental and simulation data set is available in Hu (2026) with the URL doi: http://doi.org/10.57760/sciencedb.31963.

Acknowledgments
This research was funded by the National Key Research and Development Program of China (2022YFA1604600, 2025YFF0512500), and the National Natural Science Foundation of China (42122032, 42304169). The numerical calculations in this paper have been done on the supercomputing system in the Supercomputing Center of University of Science and Technology of China.

References

Arber, T. D., Bennett, K., Brady, C. S., Lawrence-Douglas, A., Ramsay, M. G., Sircombe, N. J., et al. (2015). Contemporary particle-in-cell approach to laser-plasma modelling. *Plasma Physics and Controlled Fusion*, *57*(11), 113001. https://doi.org/10.1088/0741-3335/57/11/113001

Birn, J., Drake, J. F., Shay, M. A., Rogers, B. N., Denton, R. E., Hesse, M., et al. (2001). Geospace environmental modeling (GEM) magnetic reconnection challenge. *Journal of Geophysical Research*, *106*(A3), 3715–3719. https://doi.org/10.1029/1999JA900449

Biskamp, D. (2000). *Magnetic reconnection in plasmas*. Cambridge University Press. https://doi.org/10.1017/CBO9780511599958

Cassak, P. A., & Shay, M. A. (2012). Magnetic reconnection for coronal conditions: Reconnection rates, secondary Islands and onset. *Space Science Reviews*, *172*(1), 283–302. https://doi.org/10.1007/s11214-011-9755-2

Chang, C., Lu, Q., Lu, S., Huang, K., & Wang, R. (2024). Ion and electron motions in the outer electron diffusion region of collisionless magnetic reconnection. *Earth and Planetary Physics*, *8*(3), 472–478. https://doi.org/10.26464/epp2024020

Dai, L., Zhu, M., Ren, Y., Gonzalez, W., Wang, C., Sibeck, D., et al. (2024). Global-scale magnetosphere convection driven by dayside magnetic reconnection. *Nature Communications*, *15*(1), 639. https://doi.org/10.1038/s41467-024-44992-y

Dong, Q.-L., Wang, S.-J., Lu, Q.-M., Huang, C., Yuan, D.-W., Liu, X., et al. (2012). Plasmoid ejection and secondary current sheet generation from magnetic reconnection in laser-plasma interaction. *Physical Review Letters*, *108*(21), 215001. https://doi.org/10.1103/PhysRevLett.108.215001

Egedal, J., Fox, W., Katz, N., Porkolab, M., Reim, K., & Zhang, E. (2007). Laboratory observations of spontaneous magnetic reconnection. *Physical Review Letters*, *98*(1), 015003. https://doi.org/10.1103/PhysRevLett.98.015003

Frank, A. G. (1999). Magnetic reconnection and current sheet formation in 3D magnetic configurations. *Plasma Physics and Controlled Fusion*, *41*(3A), A687–A697. https://doi.org/10.1088/0741-3335/41/3A/062

Frank, A. G. (2025). Current sheets in plasma: From theory to experiment. *Physics-Uspekhi*, *68*(8), 823–842. https://doi.org/10.3367/UFNe.2025.03.039938

Gosling, J. T., Skoug, R. M., McComas, D. J., & Smith, C. W. (2005). Direct evidence for magnetic reconnection in the solar wind near 1 AU. *Journal of Geophysical Research*, *110*(A1). https://doi.org/10.1029/2004JA010809

Greess, S., Egedal, J., Stanier, A., Daughton, W., Olson, J., Lê, A., et al. (2021). Laboratory verification of electron-scale reconnection regions modulated by a three-dimensional instability. *Journal of Geophysical Research: Space Physics*, *126*(7), e2021JA029316. https://doi.org/10.1029/2021JA029316

Greess, S., Egedal, J., Stanier, A., Olson, J., Daughton, W., Lê, A., et al. (2022). Kinetic simulations verifying reconnection rates measured in the laboratory, spanning the ion-coupled to near electron-only regimes. *Physics of Plasmas*, *29*(10), 102103. https://doi.org/10.1063/5.0101006

Guan, Y., Lu, Q., Lu, S., Huang, K., & Wang, R. (2023). Reconnection rate and transition from ion-coupled to electron-only reconnection. *The Astrophysical Journal*, *958*(2), 172. https://doi.org/10.3847/1538-4357/ad05b8

Guan, Y., Lu, Q., Lu, S., Shu, Y., & Wang, R. (2024). Role of ion dynamics in electron-only magnetic reconnection. *Geophysical Research Letters*, *51*(19), e2024GL110787. https://doi.org/10.1029/2024GL110787

Guan, Y., Lu, Q., Lu, S., & Wang, R. (2025). Evolution of magnetic reconnection in an electron-scale current sheet. *The Astrophysical Journal*, *979*(1), 84. https://doi.org/10.3847/1538-4357/ad9b15

Hu, S. (2026). The data of the article "Electron-only magnetic reconnection in keda linear magnetized plasma (KLMP) device: Comparison between laboratory study and kinetic simulation" [Dataset]. https://doi.org/10.57760/sciencedb.31963

Huang, K., Ling, W., Tang, H., Guan, J., Yang, J., Xie, J., et al. (2025). Laboratory realization of magnetopause-like reconnection in space plasma environment research facility (SPERF). *Geophysical Research Letters*, *52*(20), e2025GL117351. https://doi.org/10.1029/2025GL117351

Hubbert, M., Qi, Y., Russell, C. T., Burch, J. L., Giles, B. L., & Moore, T. E. (2021). Electron-only tail current sheets and their temporal evolution. *Geophysical Research Letters*, *48*(5), e2020GL091364. https://doi.org/10.1029/2020GL091364

Hubbert, M., Russell, C. T., Qi, Y., Lu, S., Burch, J. L., Giles, B. L., & Moore, T. E. (2022). Electron-only reconnection as a transition phase from quiet magnetotail current sheets to traditional magnetotail reconnection. *Journal of Geophysical Research: Space Physics*, *127*(3), e2021JA029584. https://doi.org/10.1029/2021JA029584

Kleva, R. G., Drake, J. F., & Waelbroeck, F. L. (1995). Fast reconnection in high temperature plasmas. *Physics of Plasmas*, *2*(1), 23–34. https://doi.org/10.1063/1.871095

Krucker, S., Hudson, H. S., Glesener, L., White, S. M., Masuda, S., Wuelser, J.-P., & Lin, R. P. (2010). Measurements of the coronal acceleration region of a solar flare. *The Astrophysical Journal*, *714*(2), 1108–1119. https://doi.org/10.1088/0004-637X/714/2/1108

Li, C. K., Séguin, F. H., Frenje, J. A., Rygg, J. R., Petrasso, R. D., Town, R. P. J., et al. (2007). Observation of megagauss-field topology changes due to magnetic reconnection in laser-produced plasmas. *Physical Review Letters*, *99*(5), 055001. https://doi.org/10.1103/PhysRevLett.99.055001

Liu, Y.-H., Pyakurel, P., Li, X., Hesse, M., Bessho, N., Genestreti, K., & Thapa, S. B. (2025). An analytical model of "Electron-Only" magnetic reconnection rates. *Communications Physics*, *8*(1), 128. https://doi.org/10.1038/s42005-025-02034-z

Lu, Q., Fu, H., Wang, R., & Lu, S. (2022). Collisionless magnetic reconnection in the magnetosphere. *Chinese Physics B*, *31*(8), 089401. https://doi.org/10.1088/1674-1056/ac76ab

Lu, Q., Huang, C., Xie, J., Wang, R., Wu, M., Vaivads, A., & Wang, S. (2010). Features of separatrix regions in magnetic reconnection: Comparison of 2-D particle-in-cell simulations and cluster observations. *Journal of Geophysical Research*, *115*(A11). https://doi.org/10.1029/2010JA015713

Lu, Q., Shu, Y., Chang, C., Lu, S., & Wang, R. (2025). The rate of magnetic reconnection in non-steady state. *Science Bulletin*, *70*(17), 2766–2770. https://doi.org/10.1016/j.scib.2025.06.014

Lu, S., Lu, Q., Wang, R., Pritchett, P. L., Hubbert, M., Qi, Y., et al. (2022). Electron-only reconnection as a transition from quiet current sheet to standard reconnection in Earth's magnetotail: Particle-in-cell simulation and application to MMS data. *Geophysical Research Letters*, *49*(11), e2022GL098547. https://doi.org/10.1029/2022GL098547

Lu, S., Wang, R., Lu, Q., Angelopoulos, V., Nakamura, R., Artemyev, A. V., et al. (2020). Magnetotail reconnection onset caused by electron kinetics with a strong external driver. *Nature Communications*, *11*(1), 5049. https://doi.org/10.1038/s41467-020-18787-w

Ma, Z. W., & Bhattacharjee, A. (2001). Hall magnetohydrodynamic reconnection: The geospace environment modeling challenge. *Journal of Geophysical Research*, *106*(A3), 3773–3782. https://doi.org/10.1029/1999JA001004

Man, H. Y., Zhou, M., Yi, Y. Y., Zhong, Z. H., Tian, A. M., Deng, X. H., et al. (2020). Observations of electron-only magnetic reconnection associated with macroscopic magnetic flux ropes. *Geophysical Research Letters*, *47*(19), e2020GL089659. https://doi.org/10.1029/2020GL089659

Masuda, S., Kosugi, T., Hara, H., Tsuneta, S., & Ogawara, Y. (1994). A loop-top hard X-ray source in a compact solar flare as evidence for magnetic reconnection. *Nature*, *371*(6497), 495–497. https://doi.org/10.1038/371495a0

Nirwan, R., Yadav, S., Stevenson, K. J., Bartolo, G. E., Kumar, K., Cassak, P. A., & Scime, E. E. (2025). Guide-field-dependent electron acceleration during electron-only magnetic reconnection in the PHAse space MApping (PHASMA) experiment. *Physics of Plasmas*, *32*(12), 122115. https://doi.org/10.1063/5.0295902

Øieroset, M., Phan, T. D., Fujimoto, M., Lin, R. P., & Lepping, R. P. (2001). In situ detection of collisionless reconnection in the Earth's magnetotail. *Nature*, *412*(6845), 414–417. https://doi.org/10.1038/35086520

Phan, T. D., Eastwood, J. P., Shay, M. A., Drake, J. F., Sonnerup, B. U. Ö., Fujimoto, M., et al. (2018). Electron magnetic reconnection without ion coupling in Earth's turbulent magnetosheath. *Nature*, *557*(7704), 202–206. https://doi.org/10.1038/s41586-018-0091-5

Pritchett, P. L. (2001). Geospace environment modeling magnetic reconnection challenge: Simulations with a full particle electromagnetic code. *Journal of Geophysical Research*, *106*(A3), 3783–3798. https://doi.org/10.1029/1999JA001006

Pyakurel, P. S., Shay, M. A., Phan, T. D., Matthaeus, W. H., Drake, J. F., TenBarge, J. M., et al. (2019). Transition from ion-coupled to electron-only reconnection: Basic physics and implications for plasma turbulence. *Physics of Plasmas*, *26*(8), 082307. https://doi.org/10.1063/1.5090403

Rovige, L., Cruz, F. D., Dorst, R. S., Pilgram, J. J., Constantin, C. G., Vincena, S., et al. (2024). Laboratory study of magnetic reconnection in lunar-relevant mini-magnetospheres. *The Astrophysical Journal*, *969*(2), 124. https://doi.org/10.3847/1538-4357/ad4fff

Rovige, L., Cruz, F. D., Van Hoomissen, T., Dorst, R. S., Constantin, C. G., Vincena, S., et al. (2026). Direct measurement of electron heating in electron-only reconnection in a laboratory mini-magnetosphere. *Physical Review Research*, *8*(2), 023132. https://doi.org/10.1103/8ctf-q5n3

Roy, S., Bandyopadhyay, R., Matthaeus, W. H., & Pyakurel, P. S. (2024). Energy dissipation in electron-only reconnection. *The Astrophysical Journal*, *964*(1), 44. https://doi.org/10.3847/1538-4357/ad2769

Sakai, K., Moritaka, T., Morita, T., Tomita, K., Minami, T., Nishimoto, T., et al. (2022). Direct observations of pure electron outflow in magnetic reconnection. *Scientific Reports*, *12*(1), 10921. https://doi.org/10.1038/s41598-022-14582-3

Shi, P., Scime, E. E., Barbhuiya, M. H., Cassak, P. A., Adhikari, S., Swisdak, M., & Stawarz, J. E. (2023). Using direct laboratory measurements of electron temperature anisotropy to identify the heating mechanism in electron-only guide field magnetic reconnection. *Physical Review Letters*, *131*(15), 155101. https://doi.org/10.1103/PhysRevLett.131.155101

Shi, P., Srivastav, P., Barbhuiya, M. H., Cassak, P. A., Scime, E. E., & Swisdak, M. (2022a). Laboratory observations of electron heating and non-Maxwellian distributions at the kinetic scale during electron-only magnetic reconnection. *Physical Review Letters*, *128*(2), 025002. https://doi.org/10.1103/PhysRevLett.128.025002

Shi, P., Srivastav, P., Barbhuiya, M. H., Cassak, P. A., Scime, E. E., Swisdak, M., et al. (2022b). Electron-only reconnection and associated electron heating and acceleration in PHASMA. *Physics of Plasmas*, *29*(3), 032101. https://doi.org/10.1063/5.0082633

Wang, R., Cheng, Z., Slavin, J. A., Lu, Q., Raines, J., Lu, S., et al. (2024). Direct detection of ongoing magnetic reconnection at Mercury's high-latitude magnetopause. *Geophysical Research Letters*, *51*(5), e2023GL106282. https://doi.org/10.1029/2023GL106282

Wang, R., Lu, Q., Du, A., & Wang, S. (2010). In situ observations of a secondary magnetic Island in an ion diffusion region and associated energetic electrons. *Physical Review Letters*, *104*(17), 175003. https://doi.org/10.1103/PhysRevLett.104.175003

Wang, R., Lu, Q., Lu, S., Russell, C. T., Burch, J. L., Gershman, D. J., et al. (2020). Physical implication of two types of reconnection electron diffusion regions with and without ion-coupling in the magnetotail current sheet. *Geophysical Research Letters*, *47*(21), e2020GL088761. https://doi.org/10.1029/2020GL088761

Wang, R., Lu, Q., Nakamura, R., Baumjohann, W., Huang, C., Russell, C. T., et al. (2018). An electron-scale current sheet without bursty reconnection signatures observed in the near-earth tail. *Geophysical Research Letters*, *45*(10), 4542–4549. https://doi.org/10.1002/2017GL076330

Wang, R., Wang, S., Lu, Q., Li, X., Lu, S., & Gonzalez, W. (2023). Direct observation of turbulent magnetic reconnection in the solar wind. *Nature Astronomy*, *7*(1), 18–28. https://doi.org/10.1038/s41550-022-01818-5

Wang, S., Lu, S., Lu, Q., Wang, R., Ren, J., Gao, X., & Guo, J. (2024). Origin of reconnecting current sheets in shocked turbulent plasma. *Science Advances*, *10*(33), eado4639. https://doi.org/10.1126/sciadv.ado4639

Wang, Z., Vaivads, A., Fu, H. S., Cao, J. B., Lindberg, M., Turner, D. L., et al. (2023). Two-step acceleration of energetic electrons at magnetic flux ropes during turbulent reconnection. *The Astrophysical Journal*, *946*(2), 67. https://doi.org/10.3847/1538-4357/acc026

Wei, F., Hu, Q., Feng, X., & Fan, Q. (2003). Magnetic reconnection phenomena in interplanetary space. *Space Science Reviews*, *107*(1), 107–110. https://doi.org/10.1023/A:1025563420343

Yamada, M., Kulsrud, R., & Ji, H. (2010). Magnetic reconnection. *Reviews of Modern Physics*, *82*(1), 603–664. https://doi.org/10.1103/RevModPhys.82.603

Yamada, M., Ren, Y., Ji, H., Breslau, J., Gerhardt, S., Kulsrud, R., & Kuritsyn, A. (2006). Experimental study of two-fluid effects on magnetic reconnection in a laboratory plasma with variable collisionality. *Physics of Plasmas*, *13*(5), 052119. https://doi.org/10.1063/1.2203950

Yamada, M., Yoo, J., Jara-Almonte, J., Daughton, W., Ji, H., Kulsrud, R. M., & Myers, C. E. (2015). Study of energy conversion and partitioning in the magnetic reconnection layer of a laboratory plasmaa). *Physics of Plasmas*, *22*(5), 056501. https://doi.org/10.1063/1.4920960

Yang, F., Lu, Q., Zhang, Q., Xie, J., Gao, X., Ke, Y., et al. (2025). Laboratory observations of hall magnetic field in electron-only magnetic reconnection with a guide field. *Geophysical Research Letters*, *52*(7), e2024GL114151. https://doi.org/10.1029/2024GL114151

Zhang, T. L., Lu, Q. M., Baumjohann, W., Russell, C. T., Fedorov, A., Barabash, S., et al. (2012). Magnetic reconnection in the near venusian magnetotail. *Science*, *336*(6081), 567–570. https://doi.org/10.1126/science.1217013

Zhou, M., Deng, X. H., Zhong, Z. H., Pang, Y., Tang, R. X., El-Alaoui, M., et al. (2019). Observations of an electron diffusion region in symmetric reconnection with weak guide field. *The Astrophysical Journal*, *870*(1), 34. https://doi.org/10.3847/1538-4357/aaf16f